European Journal of Chemistry

View Journal Online
View Article Online

Crystallographic and Hirshfeld surface analysis of 10-(4-chlorophenyldiazenyl)-3-(3-chlorophenyl)-1-methyl-3,5a,6,11b-tetrahydro-5*H*-benzopyrano[4',3'-4,5]pyrano[2,3-c]pyrazole

Vivek Kumar Gupta [1,*], Naresh Sharma [2,*], Archna Sharma [1], Shashikant Bhikhubhai Teraiya [3], Narsidas Jeramdas Parmar [4] and Deepak Sharma [5]

[1] *Department of Physics, University of Jammu, Jammu Tawi-180006, India*
[2] *Department of Physics, Associate Professor of Physics, Government Degree College, Billawar-184204, India*
[3] *Department of Chemistry, Sheth Ranchhodlal Acharatlal College of Science, Ahmedabad-380001, Gujarat, India*
[4] *Department of Chemistry, Sardar Patel University, Vallabh Vidyanagar-388120, Gujarat, India*
[5] *Principal Boys Higher Secondary School, Reasi-182311, India*

* *Corresponding author at: Department of Physics, University of Jammu, Jammu Tawi-180006, India.*
e-mail: vivek.gupta2k9@gmail.com (V.K. Gupta), nareshbasotra@gmail.com (N. Sharma).

RESEARCH ARTICLE

10.5155/eurjchem.16.3.311-318.2668

Received: 7 February 2025
Received in revised form: 1 May 2025
Accepted: 15 June 2025
Published online: 30 September 2025
Printed: 30 September 2025

KEYWORDS

Pyrazole
Triclinic crystal system
Half-chair conformation
Hirshfeld surface analysis
Tetrahydro-5H-benzopyrano
Direct methods using single-crystal XRD

ABSTRACT

The title compound, 10-(4-chlorophenyldiazenyl)-3-(3-chlorophenyl)-1-methyl-3,5a,6,11b-tetrahydro-5*H*-benzopyrano [4',3'-4,5]pyrano[2,3-c]pyrazole, crystallizes in the triclinic crystal system having the space group *P*-1 with the following unit cell parameters: a = 7.599(2), b = 11.596(3), c = 12.796(3) Å, α = 90.092(5), β = 94.810(5), γ = 90.583(5)°, Z = 2. The crystal structure was solved by direct methods using single-crystal X-ray diffraction data collected at 100 K and refined by full-matrix least-squares procedures to a final R-value of 0.0636 for 2578 observed reflections. All three phenyl rings A, B, and F are planar. The pyrazole ring E is also planar. Rings C and D are in half-chair conformation with asymmetry parameters: ΔC_2(C7a-C11a) = 3.02 and ΔC_2(C3a-C11c) = 4.02, respectively. Hirshfeld surface is a 3D boundary around a molecule/crystal structure based on electron density. The Hirshfeld surface analysis revealed dominant H···H (31.0%), H···Cl (26%), and H···C (18%) interactions, contributing to crystal stability and packing efficiency. Molecular docking studies further indicated a strong and stable ligand-enzyme interaction, highlighting its potential for small-molecule inhibitor development.

Cite this: *Eur. J. Chem.* **2025**, *16(3)*, 311-318 **Journal website**: www.eurjchem.com

1. Introduction

For complex heterocyclic preparations [1-3], a domino strategy is a highly efficient route to assess a wide range of polycyclic compounds [4-7]. A Domino/Knoevenagel-hetero-Diels-Alder (DKHDA) approach has particularly evolved as an efficient route to many bioactive natural and unnatural compounds [8-12]. Ring systems constructed so far include chromenopyran, pyrimidonedione, tetrahydroquionoline, benzopyrano-fused benzoprane, benzopyrano-fused napthoyran and pyranoxanthene [13].

The pyrano [2,3-c] pyrazole unit has gained much prominence since it forms a central skeleton of many compounds which are known for their antimicrobial [14], insecticidal [15], anti-inflammatory [16] and molluscicidal activity [17]. Although a benzopyran ring system forms the core structure of many photochromic compounds, and is widely used in data storage, optical filters, displays, sensor protection, waveguides and ophthalmic plastic lenses [18,19], one of its classes called aminochromene is the precursor to a wide range of bioactive compounds [20-23]. Furthermore, annulations of amino-chromene with heterocycles offer an interesting and useful way to produce medicinal compounds [20-23]. Here, we wish to present the crystallographic and Hirshfeld surface analysis of 10-(4-chloro phenyldiazenyl)-3-(3-chloro phenyl)-1-methyl-3,5a,6,11b-tetrahydro-5*H*-benzopyrano[4',3'-4,5]pyrano[2,3-c]pyrazole. The chemical structure of the title compound is shown in Figure 1.

2. Experimental

2.1. Synthesis

A mixture of 2-(allyloxy)-5-((4-chlorophenyl)diazenyl) benzaldehyde (1mmol, 0.301 g), 1-(3-chlorophenyl)-3-methyl-pyrazol-5-one (1mmol, 0.208 g), and TBA-HS (tetrabutyl ammoniumhydrogensulphate) (25 mol%) was stirred in refluxing acetonitrile for 8 h [24]. After completion of the

ISSN 2153-2249 (Print) / ISSN 2153-2257 (Online)
https://dx.doi.org/10.5155/eurjchem.16.3.311-318.2668

Table 1. Crystallographic characteristics, details of the X-ray data collection, and structure refinement parameters for the title compound.

Empirical formula	$C_{26}H_{20}Cl_2N_4O_2$
Formula weight (g/mol)	491.36
Temperature (K)	293(2)
Crystal system	Triclinic
Space group	*P*-1
a (Å)	7.5994(19)
b (Å)	11.596(3)
c (Å)	12.796(3)
α (°)	90.092(5)
β (°)	94.810(5)
γ (°)	90.583(5)
Volume (Å^3)	1123.6(5)
Z	2
ρ_{calc} (g/cm^3)	1.452
μ (mm^{-1})	0.322
F (000)	508.0
Crystal size (mm^3)	0.3 × 0.2 × 0.2
Radiation	MoKα (λ = 0.71073)
2Θ range for data collection (°)	6.484 to 49.988
Index ranges	$-9 \le h \le 9, -13 \le k \le 13, -15 \le l \le 8$
Reflections collected	5755
Independent reflections	3866 [R_{int} = 0.0383, R_{sigma} = 0.0856]
Data/restraints/parameters	3866/1/319
Goodness-of-fit on F^2	0.973
Final R indexes [I≥2σ (I)]	R_1 = 0.0620, wR_2 = 0.1404
Final R indexes [all data]	R_1 = 0.0988, wR_2 = 0.1604
Largest diff. peak/hole (e.Å^{-3})	0.29/-0.24

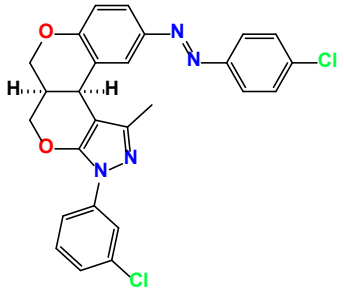

Figure 1. Chemical structure of the title compound.

reaction, as confirmed by TLC, it was cooled, and the solvent was evaporated in vacuo. The mixture was washed with acetonitrile to remove any residual starting material and dried. The product was obtained in good yield with high purity. Finally, preparative TLC was applied, using the mixture of ethyl acetate: hexane (3:7, v:v) as an eluent, to purify the product [24].

2.2. Crystal structure determination and refinement

X-ray intensity data of 5755 reflections (of which 3866 are unique) were collected on a X'calibur CCD area detector diffractometer equipped with graphite monochromated MoKα radiation (λ = 0.71073 Å). The crystal used for data collection was of dimensions 0.30×0.20×0.20 mm. The cell dimensions were determined by least-squares fit of angular settings of 3866 reflections in the θ range 2.38 to 22.34°. The intensities were measured by ϕ and ω scan mode for θ ranges 3.24 to 24.99°. 2578 reflections were treated as observed (I > 2σ(I)). Data were corrected for Lorentz, polarization, and absorption factors. All H atoms were geometrically fixed and allowed to ride on their parent C atoms with C-H = 0.93-0.98 Å. The final refinement cycles converged to *R* = 0.0636 and w*R*(F^2) = 0.1442 for the observed data. Residual electron densities ranged from -0.300 to 0.336 e.Å^{-3}. Crystal structure was solved by direct methods using SHELXS97 software [25]. A total of 256 phase sets were refined with the correct phase set having an absolute figure of merit, M(abs) = 1.109 and combined figure of merit CFOM = 0.0685. Multisolution tangent refinement was carried out using 1321 E-values with E >1.2. An E-map drawn with the correct set of phases revealed all of the non-H atoms of the molecule. The *R*-factor based on the 1321 E-values was RE = 0.187. The data were collected at 100 K. Crystal structure was solved by direct methods using SHELXS97 software [25]. Crystallographic data for the title compound are summarized in Table 1.

2.3. Hirshfeld Surface analysis

Hirshfeld surface analysis is a robust crystallographic tool that is used to quantitatively and visually assess intermolecular interactions within molecular crystals. The Hirshfeld surface is constructed on the partitioning of electron density, defining a three-dimensional boundary where the contribution of the promolecule equals that of the surrounding environment. In the present study, a Hirshfeld surface analysis was performed to investigate the nature and extent of intermolecular contacts in the crystal structure of 10-(4-chlorophenyldiazenyl)-3-(3-chloro phenyl)-1-methyl-3, 5a, 6, 11b-tetrahydro-5*H*-benzo pyrano[4′, 3′-4, 5]pyrano[2, 3-c]pyrazole. Analysis was carried out using the CrystalExplorer 21.5 software suite [26], which allows mapping of normalized contact distances (d_{norm}) on the molecular surface and generation of two-dimensional fingerprint plots. These plots provide a quantitative representation of the various types of intermolecular interactions (such as H···H, C···H, Cl···H contacts), thus providing valuable insight into the molecular packing and crystal cohesion forces that govern the solid-state structure. A detailed analysis of the Hirshfeld analysis for the present structure is provided in Section 3.3.

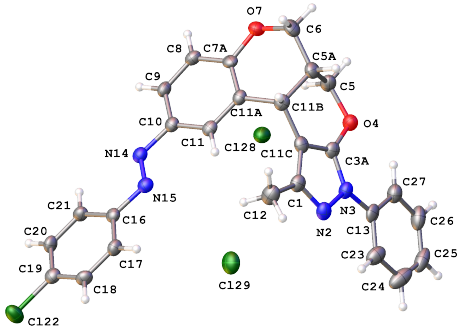

Figure 2. The structure of the compound and displacement ellipsoids are drawn at 40% probability level.

2.4. Molecular docking

Molecular docking studies for the title compound were carried out using Hex 8.0 [27], which uses spherical polar Fourier correlations to predict protein-ligand interactions efficiently. The ligand structure, derived from the experimentally determined crystal structure, was prepared using GaussView [28] and exported in pdb format without prior geometry optimization. Docking simulations were executed directly in Hex 8.0 [27] and the resulting binding energy values were obtained from the software's scoring function. No post-docking refinement or further computational analysis of the docked complexes was performed using external tools such as AutoDockTools (for flexible docking and grid-based energy evaluation) [29], Chimera (for structural visualization and hydrogen bond analysis) [30], Discovery Studio (for interaction profiling and advanced binding site analysis) [31] detailed visualization of docking poses and molecular surfaces) [32]. Additionally, no molecular dynamics (MD) simulations were performed using packages such as GROMACS or AMBER, which are commonly used to validate the stability and energetics of protein-ligand complexes in a dynamic environment.

3. Results and discussion

3.1. Synthesis

The target compound was successfully synthesized by the reaction of 2-(allyloxy)-5-((4-chlorophenyl)diazenyl) benzaldehyde and 1-(3-chlorophenyl)-3-methyl-pyrazol-5-one in the presence of tetrabutylammonium hydrogen sulfate (TBA-HS). The reaction was carried out in refluxing acetonitrile for 8 hours and its progress was monitored by thin layer chromatography (TLC), which confirmed the completion of the reaction. After solvent removal under reduced pressure and purification steps including washing with acetonitrile, the crude product was dried and isolated in good yield with high purity. Further purification was achieved by preparative TLC using an ethyl acetate:hexane (3:7, v:v) eluent system, providing the final product suitable for subsequent characterization. These results indicate that the reaction conditions employed were effective in forming the desired compound with minimal side products.

3.2. Crystal structure

The geometric parameters show normal values and are within the expected ranges (Table 2). As expected, atom N3 hybridizes with sp^2, as evidenced by the sum of the valence angles around it (360.0(2)°), with the lone pair of electrons available for bonding. The length of the N-N bond in the pyrazole ring has been reported to vary over a wide range from 1.234(8) to 1.385(4) Å, where the length depends on the substituent bonded to the N atoms; accordingly, the length of the adjacent C=N bond ranges from 1.288(4) to 1.461(8) Å. These differences are caused by a varying degree of conjugation in the electron portion of the pyrazole ring, which is sensitive to the nature of the substituent(s) bonded to the atoms of the system [33]. The N2-N3 bond length of 1.391(4) Å and C1-N2 bond length of 1.318(4)Å found in the present derivative falls in this range [33]. All three phenyl rings A, B, and F are planar.

The pyrazole ring E is also planar. Rings C and D are in half-chair conformation with asymmetry parameters: ΔC2(C7a-C11a) = 3.02 and ΔC2(C3a-C11c) = 4.02, respectively [33].

The torsion angle C21-C20-C19-Cl22 = -179.5 ° and C17-C18-C19-Cl22 = 178.5° conveys that the chlorine atom Cl22 lies almost in the plane of phenyl ring A. Additionally, the torsion angles N14-C10-C9-C8 = -180.0° and N15-C16-C21-C20 = 179.7° show that the N14 atom and N15 are almost in the plane of ring B and ring A. Furthermore, C10-N14-N15-C16 = -179.0, shows a linear character of the torsion angle. The exocyclic bond angles at the ring junction of ring B and ring C *i.e.* at C11A and C7A are 122.0(3) and 115.3(3)°, and at ring D and ring E *i.e.* at C11C and C3A are 135.6(3) and 121.2(3)°, respectively [33].

The values of the C-O bonds, (C7A-O7 = 1.367(4) Å, C6-O7 = 1.447(4) Å) in the pyran ring C and (C3A-O4 = 1.342(4) Å, C5-O4 = 1.457(4) Å) in the pyran ring D are in good agreement with the literature [33]. The bond distances C1-N2 = 1.318(4), N2-N3 = 1.391(4), C3A-N3 = 1.364(5) Å in the pyrazole ring are also in good agreement with the standard values [33].

The stability of molecules inside the unit cell is caused by intermolecular interactions of the type C-H···N, C-H···O, and C-H···π types. Table 3 provides the geometry of the C-H···N, C-H···O and C-H···π types of intermolecular hydrogen bonds. The stability of molecules inside the unit cell is caused by intermolecular interactions. Furthermore, molecules are reinforced by π···π interaction between pyrazole and phenyl rings (I and J): the distance between the ring centroids Cg1···Cg5 (1-*x*, 1-*y*, 1-*z*) is 3.937 Å; the perpendicular distance of the centroid of ring I from the plane of ring J (CgI···P is 3.219 Å); the dihedral angle between the planes of rings (α is 11°); the angle between normal to the centroid of ring I and the line joining ring centroids (β is 25.1°); and the displacement of the centroid of ring J relative to the intersection point of the normal to the ring I and the least squares plane of ring J (Δ is 2.26 Å) (Table 4).

Figure 2 shows the ORTEP view of the title compound with displacement ellipsoids drawn at 40% probability level. Crystal packing analysis revealed the presence of π-π interactions and intermolecular hydrogen bonds like C-H···N, C-H…O, and C-H···π types, all of which are crucial for stabilizing crystal structures. Figure 3 shows the packing view of molecules within the unit cell, which is created using PLATON [34] and viewed down to the *a*-axis. *Zig-zag*-like patterns are formed by the arrangement of molecules in the crystal lattice.

Table 2. Selected bond lengths, bond angles, and torsion angle for compound.

Bond	*d*, Å	Bond	*d*, Å
Cl22-C19	1.741(4)	N3-C3A	1.363(4)
N14-N15	1.261(4)	N3-N2	1.390(4)
N14-C10	1.423(4)	N3-C13	1.416(4)
O7-C7A	1.367(4)	C16-C17	1.386(5)
O7-C6	1.447(4)	C16-C21	1.397(4)
N15-C16	1.429(4)	C10-C9	1.387(5)
O4-C3A	1.344(4)	C10-C11	1.404(4)
O4-C5	1.455(4)	C17-C18	1.384(4)
C11-C11A	1.381(4)	C18-C19	1.372(5)
C11A-C7A	1.411(5)	C11A-C11B	1.526(5)
C8-C9	1.368(4)	C8-C7A	1.394(5)
N2-C1	1.319(4)	C21-C20	1.371(4)
C19-C20	1.388(5)	C11C-C3A	1.363(4)
C11C-C1	1.407(5)	C11C-C11B	1.505(5)
C11B-C5A	1.527(5)	C1-C12	1.489(5)
C13-C23	1.382(5)	C13-C27	1.400(5)
C6-C5A	1.511(5)	C5A-C5	1.518(5)
C27-C26	1.373(5)	C23-C24	1.383(5)
C25-C26	1.364(6)	C25-C24	1.382(6)
Angle	**ω, deg**	**Angle**	**ω, deg**
C3A-N3-N2	109.3(3)	C17-C16-C21	119.3(3)
C9-C10-C11	119.5(3)	C16-C17-C18	120.4(3)
C10-C11-C11A	121.5(3)	C17-C18-C19	119.4(3)
C7A-C11A-C11B	120.6(3)	C7A-C8-C9	119.7(3)
C1-N2-N3	105.2(3)	C16-C21-C20	120.6(3)
C19-C20-C21	119.3(1)	C3A-C11C-C11B	120.1(3)
C8-C7A-C11A	121-4(3)	C23-C13-C27	120.1(4)
C8-C9-C10	120.5(3)		
Torsion angle	**τ, deg**	**Angle**	**τ, deg**
C10-N14-N15-C16	-179(3)	C21-C16-C17-C18	-0.8(5)
N15-C16-C17-C18	179.4(3)	C9-C10-C11-C11A	0.3(5)
N14-C10-C11-C11A	178.8(3)	C16-C17-C18-C19	1(5)
C10-C11-C11A-C7A	1.7(5)	C1-N2-N3-C3A	0.4(9)
C17-C16-C21-C20	-0.1(5)	N15-C16-C21-C20	179.7(3)
C21-C20-C19-CL22	-179.5(3)	C17-C18-C19-CL22	178.5(3)
C21-C1-N2-N3	-176.8(3)	C1-N2-N3-C13	-171.5(3)
O4-C3A-N3-C13	-13.3(6)	C9-C10-N14-N15	-174(3)
N15-N14-C10-C11	7.4(5)	C13-C23-C24-C25	0(7)
C8-C9-C10-N14	-180(3)		

Table 3. Geometry of intermolecular interactions for a compound.

D–H···*A*	*D*–H, Å	H···*A*, Å	*D*···*A*, Å	θ(*D*–H···*A*), deg
C11-H11···N15^{i}	0.93(3)	2.517	2.770(4)	95.78(2)
C21-H21···N14^{i}	0.93(4)	2.442	2.707(5)	96.27(2)
C27-H27···O4A^{i}	0.93(4)	2.241	2.867(5)	123.99(3)
C23-H23···N2A'^{i}	0.93(4)	2.435	2.759(5)	100(2)
C6A-H61···N14^{ii}	0.97(4)	2.875	3.773(5)	154(2)
C12-H122...Cg6^{iii}	0.96	2.83	3.7143(10)	153

Symmetry codes: ^{i}*x*, *y*, z, ^{ii}1-*x*, *y*, *z*, ^{iii} -1+*x*, *y*, *z*.

Table 4. Geometry of π-π interactions for compound.

CgI	*CgJ*	*CgI*···*CgJ*, Å	*CgI*···*P*, Å	α, deg	β, deg	Δ, Å
1	5^{i}	3.937	3.219	11	25.1	2.26

Symmetry code: *i*: 1-*x*, 1-*y*, 1-*z*.

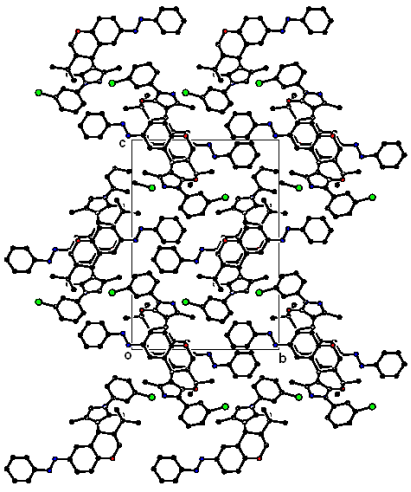

Figure 3. Packing view of molecules down to *a* axis for hydrogen interactions.

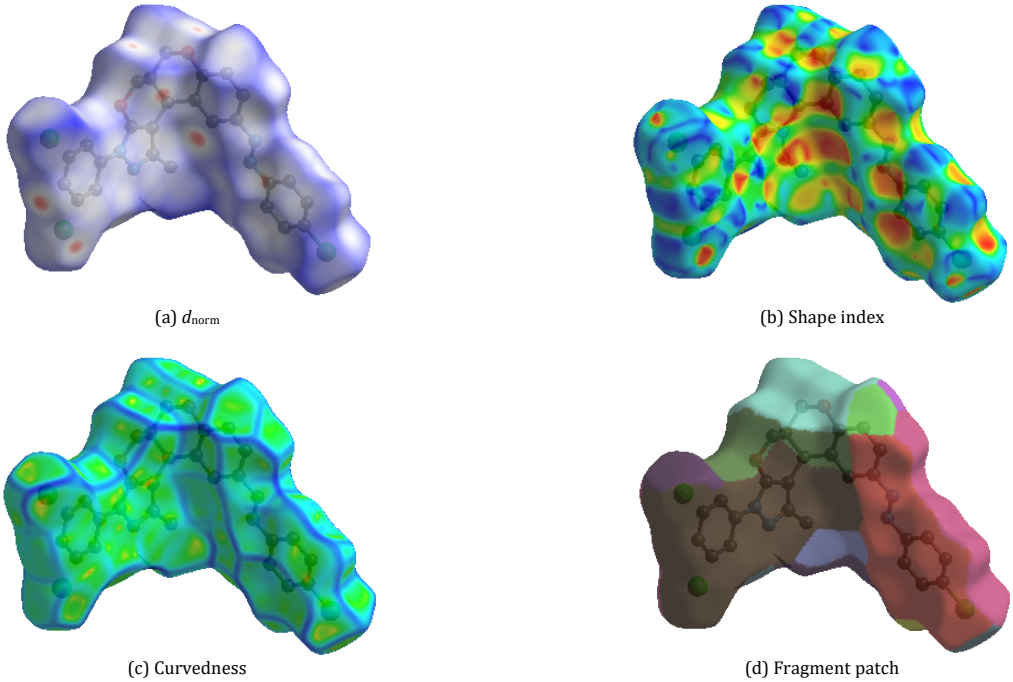

(a) d_{norm} (b) Shape index

(c) Curvedness (d) Fragment patch

Figure 4. Hirshfeld surface-mapped d_{norm}, shape index, curvedness and fragment patch for 10-(4-chlorophenyldiazenyl)-3-(3-chlorophenyl)-1-methyl-3,5a,6,11b-tetrahydro-5*H*-benzopyrano[4',3'-4,5]pyrano[2,3-c]pyrazole.

The centers of gravity of the pyrazole and phenyl rings are denoted by Cg1 and Cg5, respectively. The distance between the centroid of one ring and the plane of the other is represented by CgI···CgJ; the distance between the centroid of one ring and the plane of the other is represented by CgI···P; the dihedral angle between the planes of rings I and J is denoted by α; the angle between the normal to the centroid of ring I and the line connecting the centroids of the ring is denoted by β; the displacement of the centroid of rings J with respect to the intersection point of normal to the centroid of ring I and the least squares plane of ring J is denoted by Δ.

3.3. Hirshfeld surface analysis and Fingerprint plots

As shown in Figure 4, different aspects of the Hirshfeld surface are mapped around the given crystal structure. These aspects include normalized contact distance (d_{norm}), which is a descriptor that quantifies the strength of intermolecular interactions in a crystal structure, shape index, curvedness, and fragment patch. All these aspects help in identifying interaction sites on the given Hirshfeld surface (Figure 4). The surfaces in Figure 4 are produced in transparent mode to allow visualization of the molecular moiety in a consistent orientation. The d_{norm} range in the present case lies between -0.27 and 1.42 Å. This given range indicates the presence of strong attractive as well as repulsive interactions, thus highlighting the strength and type of interactions present; for example, the red spots in Figure 4 (d_{norm}) represent regions of closer contacts. Likewise, the red and blue regions on the shape index surface indicate concave and convex regions, respectively, thus indicating the regions that are involved in interactions between molecules in the crystal. The shape index is mapped between -0.99 and +0.99 Å. The curvedness mapped between -3.80 and 0.28 Å is the measure of the overall curvature in the Hirshfeld maps. Thus, large flat green areas indicating low curvedness values represent noninteracting sites, while sharp blue edges represent areas of close molecular interactions [35,36]. Another very important aspect of the Hirshfeld surface is the fragment patch, which aids in the understanding of crystal packing. It corresponds to regions of the Hirshfeld surface associated with a specific atom or group within the molecule. The range of the present fragment patch lies between 0.0 and 25.0 Å, indicating long range interactions. As shown in Figure 4 (Fragment patch), the different colored patches represent different molecular fragments that participate in molecular interactions with the crystal [37].

Fingerprint plots are 2D visualizations that help to understand intermolecular interactions in a crystal structure. They show how atoms or molecules in a crystal interact with their neighbors by analyzing the contact distances between them. Fingerprint plots are drawn as a function of d_i *vs.* d_e, where d_i is the distance of a point on the surface to the nearest atoms inside the surface, while d_e is the distance of a point on the surface to the nearest point outside the surface. It also gives what percentage of the surface is involved in hydrogen bonding, π-π stacking, *etc*. In Figure 5, only the dominant intermolecular interactions have been shown for the present crystal structure. Interactions that have contributions less than 5% are not shown. From Figure 5, it can be concluded that the most dominant of all interactions is the one involving H-H contacts (percentage contribution = 31.0%). The second most dominant interactions are H-Cl and H-C, which have percentage contributions of 26% and 18%, respectively. The other interactions shown in the figure are relatively smaller.

3.4. Molecular docking

Figure 6 illustrates the molecular docking interaction between the ligand 10-(4-chlorophenyldiazenyl)-3-(3-chloro phenyl)-1-methyl-3, 5a, 6, 11b-tetrahydro-5*H*-benzopyrano [4′,3′-4,5]pyrano[2,3-c]pyrazole and the biologically significant enzyme target 3HFL, which corresponds to the heme oxygenase of *Neisseria meningitidis*. Heme oxygenase enzymes catalyze the oxidative cleavage of heme to biliverdin, releasing free iron and carbon monoxide-a critical step in bacterial iron acquisition and survival under host-induced oxidative stress [38,39].

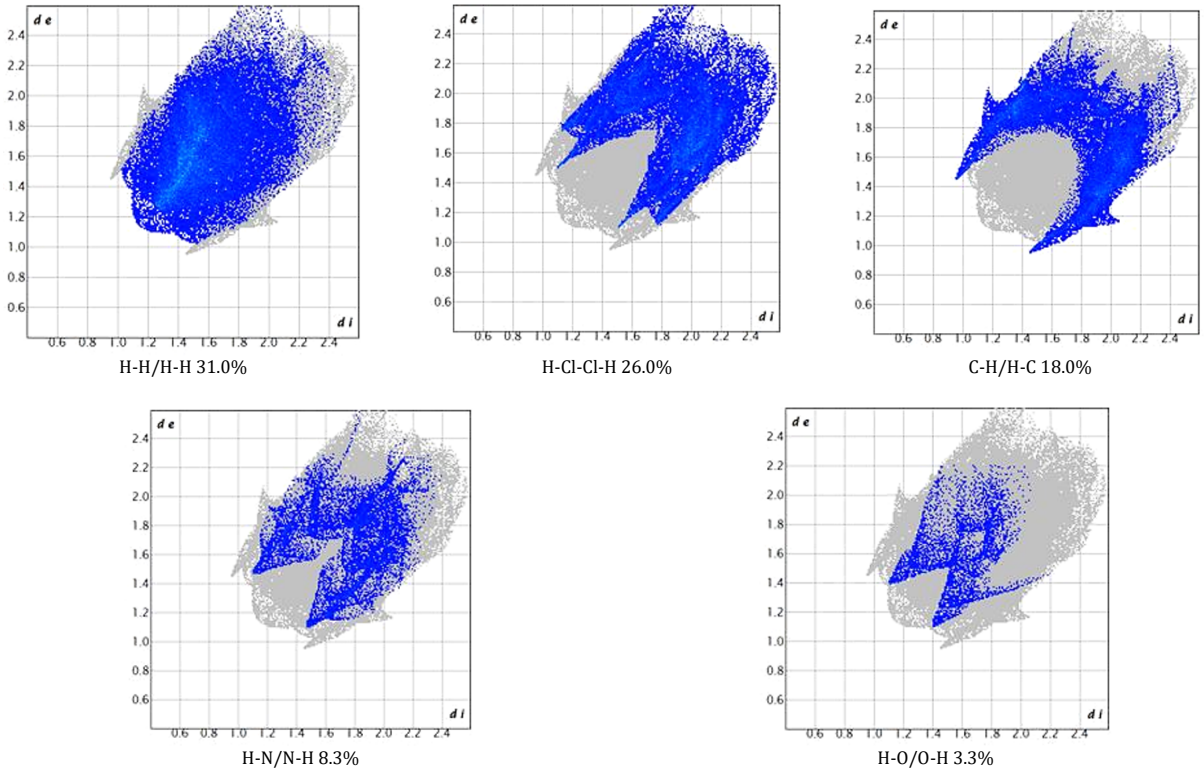

Figure 5. 2D fingerprint plots along with the percentage of surface area included, in different interactions within the given crystal structure 10-(4-chlorophenyldiazenyl)-3-(3-chlorophenyl)-1-methyl-3,5a,6,11b-tetrahydro-5*H*-benzopyrano[4',3'-4,5]pyrano[2,3-c] pyrazole.

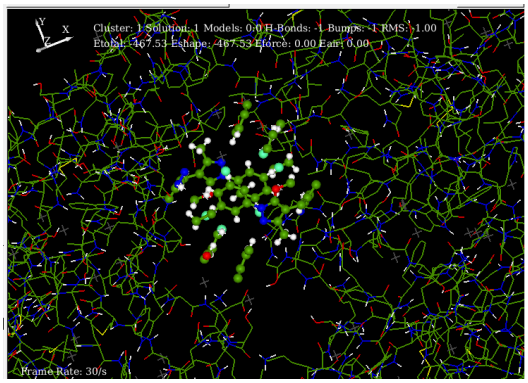

Figure 6. 10-(4-Chlorophenyldiazenyl)-3-(3-chlorophenyl)-1-methyl-3,5a,6,11b-tetrahydro-5*H*-benzopyrano[4',3'-4,5]pyrano[2,3-c]pyrazole ligand docked with 3HFL (a heme oxygenase enzyme from *Neisseria meningitides*), a target enzyme used in molecular docking studies.

Consequently, inhibition of bacterial heme oxygenases has emerged as a novel therapeutic strategy, particularly to combat antibiotic resistance in pathogenic strains such as *N. meningitidis* [40,41]. The docking simulation, performed using Hex 8.0 [42], revealed a total binding energy of -467.53 kJ/mol, suggesting a strong and energetically favorable interaction between the ligand and the enzyme. This highly negative binding energy indicates high affinity binding, likely driven by a combination of non-covalent interactions such as hydrogen bonding, hydrophobic interactions, van der Waals forces, and potential π-π stacking between the ligand's aromatic rings and the protein residues.

The structural features of the ligand-including its fused heterocyclic system and diazenyl-linked chlorophenyl moieties-contribute to its multivalent interaction profile. Halogen atoms, such as chlorine, are known to participate in halogen bonding and can improve the specificity and strength of binding by interacting with electronegative residues within the binding site [43]. Furthermore, the extended conjugated system of the ligand can allow favorable π interactions with aromatic amino acid side chains such as phenylalanine, tyrosine, or tryptophan commonly found at the active site of heme oxygenases [44].

Although the current docking study offers compelling preliminary information on the potential of the ligand as a heme oxygenase inhibitor, further analyses are required to confirm the precise interaction mechanism. Structural visualization of the binding pocket and identification of interacting residues-along with molecular dynamics (MD) simulations-would provide a more comprehensive picture of binding stability and flexibility under near-physiological conditions [45,46]. However, the significantly negative binding energy reported supports the promise of this compound as a leading scaffold for further development in the context of antimicrobial drug design targeting bacterial iron acquisition pathways.

4. Conclusions

The compound, 10-(4-chlorophenyldiazenyl)-3-(3-chloro phenyl)-1-methyl-3, 5a, 6, 11b-tetrahydro-5*H*-benzopyrano [4', 3'-4, 5]pyrano[2, 3-c]pyrazole, crystallizes in the triclinic crystal system having space group *P*-1. The pyrano[2,3-c] pyrazole unit has gained great biological importance because it is used for antimicrobial, insecticidal, anti-inflammatory and molluscicidal activity. Structure characterization of the compound was done by means of single X-ray crystallographic studies to elucidate the crystal structure and to understand the behavior of the title molecule in the presence of hydrogen bonding interactions. Different types of intermolecular interactions in the present crystal structure were studied using Hirshfeld surface analysis. Key parameters analyzed include d_{norm} (-0.27 to 1.42 Å), which highlights attractive (red spots) and repulsive interactions, shape index (-0.99 to +0.99 Å), which differentiates interaction regions, and curvedness (-3.80 to 0.28 Å), where flat green areas indicate non-interacting sites and sharp blue edges highlight close molecular interactions. Fragment patch (0.0 to 25.0 Å) maps crystal packing by associating molecular fragments with their interaction sites. These analyses provide insight into molecular stability, packing efficiency, and interaction strength within the crystal. Fingerprint plots were used to show only dominant interactions (contributions ≥ 5%) in the present case. The most significant interaction observed was H-H contacts (31.0%), followed by H-Cl (26%) and H-C (18%) interactions. Other interactions contribute relatively less to the crystal packing. These findings highlight the key forces that stabilize the crystal structure. The docking analysis indicates a strong and stable interaction between the ligand and the target enzyme, highlighting its potential as a candidate for further investigation in small-molecule inhibitor studies. The geometric parameters of the crystal structure studied fall within the expected ranges, confirming the hybridization of atom N3 with sp^2 and the influence of conjugation on the length of the bonds in the pyrazole ring. Planarity is observed in the phenyl rings (A, B, F) and the pyrazole ring (E), while rings C and D adopt a half-chair conformation. Crystal packing analysis reveals C-H···N, C-H···O, and C-H···π hydrogen bonds, along with π-π stacking interactions between the pyrazole and phenyl rings, which contribute to structural stability. The packing arrangement follows a zigzag pattern in the crystal lattice.

Acknowledgements

One of the authors (Vivek Kumar Gupta) is grateful to University of Jammu, Jammu, India, for financial support. Archna Sharma acknowledges the Department of Science and Technology, New Delhi, vide grant no. SR/WOS-A/PM-3/2018 for financial support.

Supporting information

CCDC-820933 contains the supplementary crystallographic data for this paper. These data can be obtained free of charge via https://www.ccdc.cam.ac.uk/structures/, or by e-mailing data request@ccdc.cam.ac.uk, or by contacting The Cambridge Crystallographic Data Centre, 12 Union Road, Cambridge CB2 1EZ, UK; fax: +44(0)1223-336033.

Disclosure statement

Conflict of interest: The authors declare that they have no conflict of interest.
Author contributions: All authors contributed equally to this work.
Ethical approval: All ethical guidelines have been adhered.
Sample availability: Samples of the compounds are available from the author.

CRediT authorship contribution statement

Conceptualization: Vivek Kumar Gupta, Naresh Sharma, Archna Sharma, Shashikant Bhikhubhai Teraiya, Narsidas Jeramdas Parmar and Deepak Sharma; Methodology: Vivek Kumar Gupta, Naresh Sharma, Archna Sharma, Shashikant Bhikhubhai Teraiya, Narsidas Jeramdas Parmar and Deepak Sharma; Software: Vivek Kumar Gupta, Naresh Sharma, Archna Sharma, Shashikant Bhikhubhai Teraiya, Narsidas Jeramdas Parmar and Deepak Sharma; Validation: Vivek Kumar Gupta, Naresh Sharma , Archna Sharma, Shashikant Bhikhubhai Teraiya, Narsidas Jeramdas Parmar and Deepak Sharma; Formal Analysis: Vivek Kumar Gupta, Naresh Sharma, Archna Sharma, Shashikant Bhikhubhai Teraiya, Narsidas Jeramdas Parmar and Deepak Sharma; Investigation: Vivek Kumar Gupta, Naresh Sharma, Archna Sharma, Narsidas Jeramdas Parmar; Resources: Vivek Kumar Gupta, Naresh Sharma, Archna Sharma, Shashikant Bhikhubhai Teraiya, Narsidas Jeramdas Parmar and Deepak Sharma; Data Curation: Vivek Kumar Gupta, Narsidas Jeramdas Parmar; Writing - Original Draft: Vivek Kumar Gupta, Naresh Sharma, Archna Sharma, Narsidas Jeramdas Parmar; Writing - Review and Editing: Vivek Kumar Gupta, Naresh Sharma, Archna Sharma, Narsidas Jeramdas Parmar; Visualization: Vivek Kumar Gupta, Naresh Sharma, Archna Sharma, Shashikant Bhikhubhai Teraiya, Narsidas Jeramdas Parmar and Deepak Sharma; Supervision: Vivek Kumar Gupta, Narsidas Jeramdas Parmar; Project Administration: Vivek Kumar Gupta, Narsidas Jeramdas Parmar.

ORCID and Email

Vivek Kumar Gupta
vivek.gupta2k9@gmail.com
vivekgupta@jammuuniversity.ac.in
https://orcid.org/0000-0003-2471-5943
Naresh Sharma
nareshbasotra@gmail.com
gdcbillawar2005@gmail.com
https://orcid.org/0000-0002-1128-880X
Archna Sharma
dr.archnasharma@gmail.com
https://orcid.org/0000-0002-4634-7486
Shashikant Bhikhubhai Teraiya
sbteraiya@gmail.com
https://orcid.org/0000-0003-2960-3967
Narsidas Jeramdas Parmar
njpchemdeptspu@yahoo.co.in
https://orcid.org/0000-0003-4580-7249
Deepak Sharma
dpkshrmajmu@gmail.com
https://orcid.org/0009-0004-3867-6468

References

[1]. Nicolaou, K. C.; Snyder, S. A.; Montagnon, T.; Vassilikogiannakis, G. The Diels--Alder Reaction in Total Synthesis. *Angew. Chem. Int. Ed Engl.* **2002**, 41 (10), 1668–1698.
[2]. Matiychuk, V. S.; Lesyk, R. B.; Obushak, M. D.; Gzella, A.; Atamanyuk, D. V.; Ostapiuk, Y. V.; Kryshchyshyn, A. P. A new domino-Knoevenagel–hetero-Diels–Alder reaction. *Tetrahedron Lett.* **2008**, *49* (31), 4648–4651.
[3]. Bryhas, A. O.; Horak, Y. I.; Ostapiuk, Y. V.; Obushak, M. D.; Matiychuk, V. S. A New Three-Step Domino Knoevenagel–Hetero-Diels–Alder Oxidation Reaction. *Tetrahedron Lett.* **2011**, *52* (18), 2324–2326.
[4]. Tietze, L. F. Domino Reactions in Organic Synthesis. *Chem. Rev.* **1996**, *96* (1), 115–136.
[5]. Tietze, L. F.; Beifuss, U. Sequential Transformations in Organic Chemistry: A Synthetic Strategy with a Future. *Angew. Chem. Int. Ed. Engl.* **1993**, *32* (2), 131–163.
[6]. Zhang, Z.; Zhang, Q.; Sun, S.; Xiong, T.; Liu, Q. Domino Ring-Opening/Recyclization Reactions of Doubly Activated Cyclopropanes as a Strategy for the Synthesis of Furoquinoline Derivatives. *Angew. Chem. Int. Ed.* **2007**, *46* (10), 1726–1729.
[7]. Yadav, A. K.; Peruncheralathan, S.; Ila, H.; Junjappa, H. Domino Carbocationic Rearrangement of α-[Bis(methylthio)methylene]alkyl-2-(3/2-indolyl) Cyclopropyl Ketones. *J. Org. Chem.* **2007**, *72* (4), 1388–1394.
[8]. Pellissier, H. Asymmetric domino reactions. Part B: Reactions based on the use of chiral catalysts and biocatalysts. *Tetrahedron* **2006**, *62* (10), 2143–2173.
[9]. Ceulemans, E.; Voets, M.; Emmers, S.; Uytterhoeven, K.; Van Meervelt, L.; Dehaen, W. Diastereoselective Intramolecular Hetero Diels–Alder Approach towards Polycyclic Heterocycles. *Tetrahedron* **2002**, *58* (3), 531–544.
[10]. Dat, N. T.; Lee, J.; Lee, K.; Hong, Y.; Kim, Y. H.; Lee, J. J. Phenolic Constituents of *Amorpha fruticosa* That Inhibit NF-κB Activation and Related Gene Expression. *J. Nat. Prod.* **2008**, *71* (10), 1696–1700.

[11]. Snider, B. B.; Lu, Q. Total Synthesis of (.+-.)-Pyridoxatin. *J. Org. Chem.* **1994**, *59* (26), 8065–8070.
[12]. Majumdar, K.; Taher, A.; Ray, K. Domino-Knoevenagel-hetero-Diels–Alder reactions: an efficient one-step synthesis of indole-annulated thiopyranobenzopyran derivatives. *Tetrahedron Lett.* **2009**, *50* (27), 3889–3891.
[13]. Lee, Y. R.; Kim, Y. M.; Kim, S. H. Efficient one-pot synthesis of benzopyranobenzopyrans and naphthopyranobenzopyrans by domino aldol-type reaction/hetero Diels–Alder reaction of resorcinols and naphthols. *Tetrahedron* **2009**, *65* (1), 101–108.
[14]. El-Tamany, E. S.; El-Shahed, F. A.; Mohamed, B. H. Synthesis and biological activity of some pyrazole derivatives. *J. Serbian Chem. Soc.* **1999**, *64* (1), 9–19.
[15]. Ismail, Z. H.; Aly, G. M.; El-Degwi, M. S.; Heiba, H. I.; Ghorab, M. M. Synthesis and insecticidal activity of some new pyranopyrazoles, pyrazolopyranopyrimidines, and pyrazolopyranopyridines. *Egypt. J. Biotechnol.* **2003**, *13*, 73–82.
[16]. Zaki, M. E.; Soliman, H. A.; Hiekal, O. A.; Rashad, A. E. Pyrazolopyranopyrimidines as a Class of Anti-Inflammatory Agents. *Zeitschrift Naturforschung. C* **2006**, *61* (1-2), 1–5.
[17]. Abdelrazek, F. M.; Metz, P.; Kataeva, O.; Jäger, A.; El-Mahrouky, S. F. Synthesis and Molluscicidal Activity of New Chromene and Pyrano[2,3-c]Pyrazole Derivatives. *Arch. Pharm. (Weinheim)* **2007**, *340* (10), 543–548.
[18]. Photochromism: Molecules and Systems, 2nd ed.; Durr, H., Bouas-Laurent, H., Eds.; Elsevier Science: London, England, 2003.
[19]. Organic Photochromic and Thermochromic Compounds: Main Photochromic Families, 1999th ed.; Crano, J. C., Guglielmetti, R. J., Eds.; Kluwer Academic/Plenum: New York, NY, 1999.
[20]. Mannhold, R.; Cruciani, G.; Weber, H.; Lemoine, H.; Derix, A.; Weichel, C.; Clementi, M. 6-Substituted Benzopyrans as Potassium Channel Activators: Synthesis, Vasodilator Properties, and Multivariate Analysis. *J. Med. Chem.* **1999**, *42* (6), 981–991.
[21]. Brown, C. W.; Liu, S.; Klucik, J.; Berlin, K. D.; Brennan, P. J.; Kaur, D.; Benbrook, D. M. Novel Heteroarotinoids as Potential Antagonists of *Mycobacteriumbovis* BCG. *J. Med. Chem.* **2004**, *47* (4), 1008–1017.
[22]. Parmar, N. J.; Teraiya, S. B.; Patel, R. A.; Talpada, N. P. Tetrabutylammonium Hydrogen Sulfate Mediated Domino Reaction: Synthesis of Novel Benzopyran-Annulated Pyrano[2,3-c]Pyrazoles. *Tetrahedron Lett.* **2011**, *52* (22), 2853–2856.
[23]. Conti, C.; Desideri, N. New 4H-Chromen-4-One and 2H-Chromene Derivatives as Anti-Picornavirus Capsid-Binders. *Bioorg. Med. Chem.* **2010**, *18* (17), 6480–6488.
[24]. Parmar, N. J.; Teraiya, S. B.; Patel, R. A.; Talpada, N. P. Tetrabutylammonium Hydrogen Sulfate Mediated Domino Reaction: Synthesis of Novel Benzopyran-Annulated Pyrano[2,3-c]Pyrazoles. *Tetrahedron Lett.* **2011**, *52* (22), 2853–2856.
[25]. Sheldrick, G. M. Crystal structure refinement with *SHELXL*. *Acta. Crystallogr. C. Struct. Chem.* **2015**, *71* (1), 3–8.
[26]. Spackman, P. R.; Turner, M. J.; McKinnon, J. J.; Wolff, S. K.; Grimwood, D. J.; Jayatilaka, D.; Spackman, M. A. CrystalExplorer: a program for Hirshfeld surface analysis, visualization and quantitative analysis of molecular crystals. *J. Appl. Crystallogr.* **2021**, *54*, 1006–1011.
[27]. Ritchie, D. W.; Kemp, G. J. Protein Docking Using Spherical Polar Fourier Correlations. *Proteins* **2000**, *39* (2), 178–194.
[28]. Dennington, R.; Keith, T. A.; Millam, J. M. GaussView, Version 6, Semichem Inc.; Shawnee Mission, KS, 2016.
[29]. Morris, G. M.; Huey, R.; Lindstrom, W.; Sanner, M. F.; Belew, R. K.; Goodsell, D. S.; Olson, A. J. AutoDock4 and AutoDockTools4: Automated docking with selective receptor flexibility. *J. Comput. Chem.* **2009**, *30* (16), 2785–2791.
[30]. Pettersen, E. F.; Goddard, T. D.; Huang, C. C.; Couch, G. S.; Greenblatt, D. M.; Meng, E. C.; Ferrin, T. E. UCSF Chimera—A visualization system for exploratory research and analysis. *J. Comput. Chem.* **2004**, *25* (13), 1605–1612.
[31]. BIOVIA, Dassault Systemes. Discovery Studio Visualizer, v20.1.0.19295; Dassault Systemes: San Diego, 2020.
[32]. Schrödinger, LLC. The PyMOL Molecular Graphics System, Version 2.0; Schrödinger, LLC: New York, 2015.
[33]. Allen, F. H.; Kennard, O.; Watson, D. G.; Brammer, L.; Orpen, A. G.; Taylor, R. Tables of bond lengths determined by X-ray and neutron diffraction. Part 1. Bond lengths in organic compounds. *J. Chem. Soc., Perkin. Trans. 2* **1987**, S1.
[34]. Spek, A. L. Structure validation in chemical crystallography. *Acta. Crystallogr. D. Biol. Crystallogr.* **2009**, *65* (2), 148–155.
[35]. McKinnon, J. J.; Jayatilaka, D.; Spackman, M. A. Towards quantitative analysis of intermolecular interactions with Hirshfeld surfaces. *Chem. Commun.* **2007**, 3814.
[36]. Matsuno, T.; Sato, S.; Isobe, H. Curved π-Receptors. *Comprehensive Supramolecular Chemistry II* **2017**, 311–328.
[37]. Harchani, A.; Haddad, A. Application of Hirshfeld surfaces, semiempirical calculations and molecular dynamics analysis to study the intermolecular interactions, reactivity and dynamics of two polyoxometalate compounds. *Theor. Chem. Acc.* **2018**, *137* (7), https://doi.org/10.1007/s00214-018-2279-z.
[38]. Ortiz de Montellano, P. R.; Wilks, A. Heme Oxygenase Structure and Mechanism. In Advances in Inorganic Chemistry; Elsevier, 2000; pp 359–407.
[39]. Skaar, E. P. The Battle for Iron between Bacterial Pathogens and Their Vertebrate Hosts. *PLoS. Pathog.* **2010**, *6* (8), e1000949.
[40]. Létoffé, S.; Heuck, G.; Delepelaire, P.; Lange, N.; Wandersman, C. Bacteria Capture Iron from Heme by Keeping Tetrapyrrol Skeleton Intact. *Proc. Natl. Acad. Sci. U. S. A.* **2009**, *106* (28), 11719–11724.
[41]. Lansky, I. B.; Lukat-Rodgers, G. S.; Block, D.; Rodgers, K. R.; Ratliff, M.; Wilks, A. The Cytoplasmic Heme-Binding Protein (PhuS) from the Heme Uptake System of Pseudomonas Aeruginosa Is an Intracellular Heme-Trafficking Protein to the Delta-Regioselective Heme Oxygenase. *J. Biol. Chem.* **2006**, *281* (19), 13652–13662.
[42]. Ritchie, D. W.; Venkatraman, V. Ultra-fast FFT protein docking on graphics processors. *Bioinformatics* **2010**, *26* (19), 2398–2405.
[43]. Wilcken, R.; Zimmermann, M. O.; Lange, A.; Joerger, A. C.; Boeckler, F. M. Principles and Applications of Halogen Bonding in Medicinal Chemistry and Chemical Biology. *J. Med. Chem.* **2013**, *56* (4), 1363–1388.
[44]. McGaughey, G. B.; Gagné, M.; Rappé, A. K. π-Stacking Interactions. *Journal of Biological Chemistry* **1998**, *273* (25), 15458–15463.
[45]. Hollingsworth, S. A.; Dror, R. O. Molecular Dynamics Simulation for All. *Neuron* **2018**, *99* (6), 1129–1143.
[46]. Durrant, J. D.; McCammon, J. A. Molecular dynamics simulations and drug discovery. *BMC. Biol.* **2011**, *9* (1), https://doi.org/10.1186/1741-7007-9-71.